Received 21 January 2020; accepted 11 February 2020. Date of publication 14 February 2020; date of current version 26 February 2020.
The review of this article was arranged by Editor E. Sangiorgi.

Digital Object Identifier 10.1109/JEDS.2020.2974031

A Mobility Model Considering Temperature and Contact Resistance in Organic Thin-Film Transistors

NA LI[1], WANLING DENG[1], WEIJING WU[2], ZHI LUO[1], AND JUNKAI HUANG[1]

1 Department of Electronic Engineering, Jinan University, Guangzhou 510630, China
2 State Key Laboratory of Luminescent Materials and Devices, South China University of Technology, Guangzhou 510640, China

CORRESPONDING AUTHOR: W. DENG (e-mail: dwanl@126.com)

This work was supported in part by the Guangdong Natural Science Foundation under Grant 2018A030313018, in part by the Fundamental Research Funds for the Central Universities under Grant D2190970, and in part by the National Natural Science Foundation of China under Grant 61874046.

ABSTRACT Based on the device physics, a mobility model for organic thin-film transistors (OTFTs) is presented considering temperature and contact resistance. As a function of the surface potential, the mobility model including hopping mechanism is able to explain the dependence of temperature and gate bias. The contact resistance is also considered in order to extract the correct mobility. Furthermore, with the assumption that the trapped carrier concentration dominates Poisson's equation, and combining the mobility model, a DC compact model accounting for contact resistance and temperature is proposed suitable for the temperature scaling from 83 to 295K. Through the extensive comparisons between the model results and the numerical iteration or experimental data, the validity of the mobility and current models is strongly supported.

INDEX TERMS Mobility model, organic thin-film transistors, temperature, contact resistance, hopping, DC model.

I. INTRODUCTION

Recently, organic thin-film transistors (OTFTs) have received a great intention due to their applications in large-area devices, large-scale complementary integrated circuits, driving circuits for flat panel displays, memory components for transaction cards, smart cards, identification cards and various gas sensors [1]–[3]. For further applications of OTFTs, a poor mobility is the main obstacle, and it can be several orders of magnitude smaller than that of conventional semiconductors [4]. Thus, it is of crucial importance to understand the carrier transport properties in these organic materials for designing and synthesizing better materials and devices.

Over these years, several mobility models have been reported to describe the characteristics of OTFTs [5]–[12]. Mott [5] first analyzed the jumping process of carriers between trap states in amorphous materials, and proposed the mechanism of variable range hopping (VRH). Horowitz *et al.* [6] and Servati *et al.* [7] explained the relationship between mobility and temperature based on the multiple trap and release (MTR) in organic semiconductors. Maiti *et al.* [8]–[10] summarized several carrier transport mechanisms and developed a physical-based compact mobility model as a function of surface potential. However, it did not study the temperature characteristic of OTFTs. Kim *et al.* [11] reported a high mobility OTFT, and they found that the carrier transport mechanism varied from VRH or Gaussian disorder-based model (GDM) to MTR, depending on the operating temperature. Liu *et al.* [12] reviewed various carriers transport mechanisms in OTFTs and explained the relationship between mobility and temperature for OTFTs in different channel materials. Nevertheless, the influence of contact resistance is not taken into account in these models. It should be noted that mobility in transistors with gated Schottky contact can be overestimated by more than 10 times [13], and therefore, the contact has a significant effect on an OTFT. The contact effect decreases the effective drain-source and gate-source voltages applied to the intrinsic channel, thus reducing the device current. In order to accurately reproduce the behaviors of mobility and

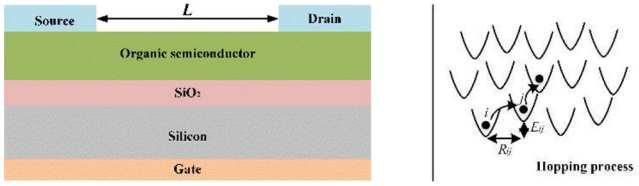

FIGURE 1. **(a) Structure of an OTFT and (b) hopping taking place between two neighboring localized states [10].**

drain current, the inclusion of contact resistance becomes very necessary.

In this paper, we present a compact mobility model as a function of temperature for OTFTs. Based on the Miller-Abrahams rate equation and the Einstein diffusion relation, we discuss the dependence of mobility on surface potential and temperature. Since the contact resistance strongly affects the mobility, we calculate it and extract the exact mobility. Finally, combining the mobility and drain current models, a DC compact model considering contact resistance and temperature is proposed with temperature scaling from 83 to 295K. The calculated drain current is verified by available experimental data at different temperatures.

II. THE HOPPING MOBILITY MODEL

The cross-section view of an OTFT is shown in Fig. 1(a). The source and the drain locate at the top side, the gate is at the bottom side, and an organic semiconductor (OSC) layer exists in between the gate oxide and the source/drain. Note that, in OTFTs, the highest occupied molecular orbital (HOMO) is similar to the valence band in silicon, and the lowest unoccupied molecular orbital (LUMO) is similar to the conduction band [14]. The energy difference between them is the bandgap energy (E_g), in which the conduction is sophisticated and takes place by carrier hopping between two neighboring localized states as shown in Fig. 1(b) [10].

In organic semiconductor, the disorder in the molecular arrangement and the presence of grain boundaries lead to the high density of localized states. Based on [10], we obtain the hopping mobility (μ_{HOP}) equation as

$$\mu_{HOP} = \frac{3\nu_0\beta B}{4\pi R_{ij} N_{t0}} \exp\left(\frac{E_f - E_t}{kT}\right) \tag{1}$$

where ν_0 is the hopping frequency; $\beta = q/kT$; q is the elementary charge; k is the Boltzmann constant; T is the absolute temperature; $B \approx 2.7 \pm 0.1$ is the percolation threshold; R_{ij} is the average jumping distance; N_{t0} is the occupied localized charge concentration; E_f is the Fermi energy level; and E_t is the transport energy. Notice that, N_{t0} is a constant in [10], but herein, it should be expressed as [15]

$$\begin{aligned} N_{t0} &= \int_{E_i}^{\infty} g(E) f(E) dE \\ &= \frac{g_2 \pi kT}{sin\frac{\pi T}{T_2}} \exp\left(\frac{E_{f0}}{kT_2}\right) \exp\left(\frac{\varphi - V_{ch}}{kT_2/q}\right) \end{aligned} \tag{2}$$

where $g(E)$ is the density of states (DOS) at localized energy (E); $f(E)$ is the Fermi-Dirac function; g_2 is the tail DOS at E_{LUMO}; E_{LUMO} is the LUMO energy; $E_{f0} = E_f - E_{LUMO}$ in the neutral organic thin-film [16]; V_{ch} is the channel potential respect to the source; and T_2 is the distribution function width. Therefore, inserting (2) into (1), the hopping mobility is

$$\mu_{HOP} = \frac{3\nu_0\beta B}{4\pi R_{ij}} \frac{sin\frac{\pi T}{T_2}}{g_2 \pi kT} \exp\left(\frac{E_f - E_t}{kT} - \frac{(\varphi - V_{ch})q + E_{f0}}{kT_2}\right). \tag{3}$$

From Eq. (3), we know that μ_{HOP} is a function of energy ($E_f - E_t$). Therefore, we transform $E_f - E_t$ into [8]

$$E_f - E_t = q\varphi_s + E_{f0} - \frac{E_g}{2}, \tag{4}$$

where φ_s is the surface potential; $E_g = E_{HOMO} - E_{LUMO}$ and it is the bandgap of the OSC; and E_{HOMO} is the HOMO energy. In this paper, as the term of ($sin\frac{\pi T}{T_2}$) changes from 0.5 to 1, the impact on temperature is insignificant. Therefore, we consider M_1 ($M_1 = \frac{3\nu_0\beta B}{4\pi R_{ij}} \frac{sin\frac{\pi T}{T_2}}{g_2\pi k}$) as a model parameter. Given that the surface-potential-based DC model is described in the following section, the mobility is also expressed by surface potential, making the relationship between mobility and electrical field more straightforward. Thus, we rewrite the μ_{HOP} equation as

$$\mu_{HOP} = \frac{M_1}{T} \exp\left(\frac{q\varphi_s + E_{f0} - E_g/2}{kT} - \frac{(\varphi_s - V_{ch})q + E_{f0}}{kT_2}\right). \tag{5}$$

The above equation shows temperature-dependent hopping mobility as $\log(\mu T) \propto T^{-1}$ and surface-potential-dependent mobility as $\log(\mu) \propto \varphi_s$. When E_f is located at different energy, the deep and tail state densities dominate respectively the subthreshold and above-threshold characteristics. As a consequence, we divide the mobility model into two regimes. In different regimes, the mobility can be simplified as

$$\mu_R = \frac{MA}{T} \exp\left(\frac{MB_R}{T} + MC_R\varphi_s\right) \tag{6}$$

where μ_R represents μ_{sub} and μ_{ab}, respectively. Likewise, MB_R and MC_R represent MB_{sub}, MB_{ab} and MC_{sub}, MC_{ab}, respectively. The subscript R means parameters restricted in the corresponding regimes. The subscripts *sub* and *ab* denote the subthreshold and above-threshold regimes, respectively.

Consequently, the proposed semi-empirical mobility (μ_{eff}) formulation for OTFTs takes on the following form [17]

$$\mu_{eff} = \frac{\mu_{sub}}{1 + \exp(m_0 V_{gt})} + \frac{\mu_{ab}}{1 + \exp(-m_0 V_{gt})} \tag{7}$$

where m_0 is a fitting parameter for the connection of μ_{sub} and μ_{ab}; $V_{gt} = V_{gs} - V_T$, and V_{gs} is the gate-to-source voltage; V_T is the threshold voltage, which is extracted at the x-axis intercept of the transfer characteristic in the above-threshold regime [11].

TABLE 1. Simulation parameters used in Figs. 2-7.

Parameter	[29]	[30]	[31]
$W(\mu m)$	2×10^4	1×10^4	200
$L(\mu m)$	10	5	10
$C_{ox}(nF/cm^2)$	15	17	2.71
$g_1(cm^{-3}eV^{-1})$	1×10^{18}	2×10^{18}	1×10^{16}
$E_1(eV)$	0.12	0.12	0.12
$g_2(cm^{-3}eV^{-1})$	6×10^{20}	2.6×10^{21}	1.1×10^{19}
$E_2(eV)$	0.03	0.03	0.03
$D(-)$	1	1	1
$a_1(-)$	0.2	0.2	0.2
$a_2(-)$	0.1	0.1	0.1
$R_{00}(\Omega)$	3936	4273	4.4×10^5
$R_m(K)$	2089	1115	940
MB_{sub} (K)	-9000	-9600	-9300
$MC_{sub}(V^{-1})$	10	23	30
$MB_{ab}(K)$	-2630	-1380	-1250
$MC_{ab}(V^{-1})$	8	6.5	8

III. THE EXTRACTION OF MEASURED MOBILITY

All the parameters in the mobility model are summarized in Table 1. To include the contact effect in the mobility model and determine the parameters in (6), the extraction procedure is divided into two steps as described in the following.

A. FIRST STEP

Extraction of the measured mobility (μ_m) and contact resistance (R_C).

To acquire the measured mobility, we can first extract the field-effect mobility from the transconductance [11], [18]

$$\mu_{m1} = \frac{L}{WC_{ox}V_{ds}}\frac{\partial I_{ds}}{\partial V_{gs}} \tag{8}$$

where L and W are the channel length and width of transistors, respectively; C_{ox} is the gate insulator capacitance; I_{ds} and V_{ds} are the drain-to-source current and voltage, respectively. The term $\frac{\partial I_{ds}}{\partial V_{gs}}$ is obtained directly from the transfer curve.

Nevertheless, Eq. (8) holds only when contact resistance can be neglected according to [13]. As mentioned above, it is necessary to consider the contact effect into mobility in OTFTs. Therefore, the following simple equation [19] can be used to include R_C

$$\mu_m = \frac{\mu_{m1}R_{ch}}{R_C + R_{ch}} \tag{9}$$

where $R_{ch} = R_T - R_C$ and it is the channel resistance; $R_T = V_{ds}/I_{ds}$ and it is the total resistance. The contact resistance (R_C) can be expressed as [13]

$$R_C = R_0\exp\left(-D\left|V_{gs}\right|^{a_1}\right){V_{gs}}^{a_2} \tag{10}$$

where $R_0 = R_{00}\exp(\frac{R_m}{T})$; D, a_1, and a_2 are characteristic parameters determined by materials and device structures; R_{00} and R_m are tuned to fit R_0. As a result, the measured mobility (μ_m) considering the contact resistance can finally be calculated from Eqs. (9) and (10).

B. SECOND STEP

Extraction of MA, MB_R, and MC_R.

After Step 1, by making the fitting parameters in Eq. (6) consistent with the extracted mobility (μ_m), our proposed mobility model in (6) takes the contact effect into account.

For more details, firstly, MA is set to be 1 $cm^2\cdot K/Vs$. After μ_m is determined, the plots of $\log(\mu_m T)$ vs. T^{-1} for different gate bias can be obtained. Secondly, as described in [20], from the subthreshold swing, the deep state density parameters of g_1 and E_1 can be extracted. Then φ_s can be computed as shown in Section IV. Thirdly, initial values of MB_R and MC_R are estimated from the slopes of $\log(\mu_m T)$ vs. T^{-1} and $\log(\mu_m)$ vs. φ_s lines, respectively. Then, MB_R and MC_R are also optimized to fit the plot of $\log(\mu)$ vs. V_{gs} in the subthreshold and above-threshold regimes at different temperatures, respectively.

IV. THE COMPACT DC MODEL

In OTFTs, the energy disorder is usually described by the double exponential distributions as [21]–[24]:

$$g(E) = g_1\exp\left(\frac{E - E_{LUMO}}{kT_1}\right) + g_2\exp\left(\frac{E - E_{LUMO}}{kT_2}\right) \tag{11}$$

where T_1 is the distribution function width.

Following our previous work [25], in the subthreshold regime, according to the Lambert W function (W_0), the surface potential yields

$$\varphi_{sub} = V_{gs} - V_{fb} - 2\phi_1 W_0\left[\frac{\sqrt{2q\varepsilon_s N_1\phi_1}}{2\phi_1 C_{ox}}\exp\left(\frac{V_{gs} - V_{fb} - V_{ch}}{2\phi_1}\right)\right]. \tag{12}$$

In the above-threshold regime, we can also get

$$\varphi_{ab} = V_{gs} - V_{fb} - 2\phi_2 W_0\left[\frac{\sqrt{2q\varepsilon_s N_2\phi_2}}{2\phi_2 C_{ox}}\exp\left(\frac{V_{gs} - V_{fb} - V_{ch}}{2\phi_2}\right)\right]. \tag{13}$$

All parameter definitions can be referred to [26]. Applying the smoothing function to (12) and (13), one obtains the surface potential φ_s.

The drain current reads [27]

$$I_{ds} = \frac{\mu_{eff}W}{L}\int_0^{V_{ds}} Q_a dV_{ch} \tag{14}$$

where Q_a is the accumulation charge per unit area at the semiconductor-insulator interface, i.e.,

$$Q_a = q\int_{V_{ch}}^{\varphi_s}\frac{n_t(\varphi, V_{ch})}{E(\varphi, V_{ch})}d\varphi. \tag{15}$$

It can be approximated as

$$Q_a = N_2\sqrt{\frac{q\varepsilon_s}{2}}\exp\left(\frac{\varphi_s - V_{ch}}{\phi_t}\right)\Bigg/\Bigg[N_1\phi_1\left(\frac{1}{\phi_t} - \frac{1}{2\phi_1}\right)^2 \exp\left(\frac{\varphi_s - V_{ch}}{\phi_1}\right) + N_2\phi_2\left(\frac{1}{\phi_t} - \frac{1}{2\phi_2}\right)^2\exp\left(\frac{\varphi_s - V_{ch}}{\phi_2}\right)\Bigg]^{\frac{1}{2}}. \tag{16}$$

Thus, we combine the mobility model (7) into the current model to obtain the final drain current expression as

$$I_{ds} = I_{Deep} + I_{Tail} \tag{17}$$

where the current components considering the deep state density (I_{Deep}) and the tail state density (I_{Tail}) are given by (18), as shown at the bottom of this page and (19), as shown at the bottom of this page, respectively.

Note that, in [26], the free electron charge contributes to the drain current. However, as discussed in [18], [27], since hopping mechanism is dominated in OTFTs, both the trapped carrier concentration and the accumulation charge are the contribution components for drain current. In addition, the current model [26] is only satisfied when the mobility is larger than 0.1 cm^2/Vs. Our model results indicate that the value of mobility is not a constant, but dependent on the temperature and surface potential. Furthermore, our mobility model also considers the contact resistance, which is not taken into account by [26]. Hence, the physical-based mobility model of (5) is more suitable and precise for the drain current model of (17). Combining the mobility model with the drain current, a good fitting result verifies the effectiveness. As a result, a surface-potential-based drain current model (17) is developed considering both deep and tail DOS for OTFTs.

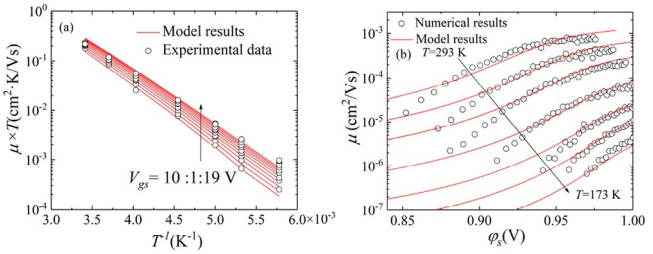

FIGURE 2. Plots of (a) log(μT) vs. T^{-1} for different gate bias, with intervals of 1 V and (b) log(μ) vs. φ_s at different temperatures, and the temperatures in the direction of the arrow are 293, 270, 248, 220, 200, 188, 173K.

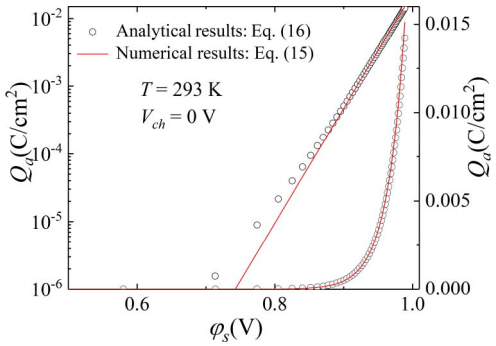

FIGURE 3. The accumulation charge per unit area at the semiconductor-insulator interface (Q_d) variation along with φ_s.

V. RESULTS AND DISCUSSIONS

As depicted in Fig. 2(a), the measured mobility can be extracted by (9) at different V_{gs} to show the hopping mechanism described by (5), where the y-axis is the mobility times T, and the x-axis is the units of T^{-1}. It can be seen that, even though at high V_{gs}, the hopping mechanism still dominates. In Fig. 2(b), the mobility is plotted as a function of φ_s, where a good fit at high φ_s can be seen.

From the linear and semi-logarithmic coordinates of Fig. 3, it can be seen that the analytical results (16) accurately represent the numerical results (15), which well implies the precision of Eq. (16) as the approximation of (15). Based on Liu *et al.* [13], [28], the contact resistance is related to V_{gs}, and it can be calculated by Eq. (10). Figure 4 shows the channel and contact resistances as a function of V_{gs}. It indicates that R_C is comparable to R_{ch} at high V_{gs}, and therefore, taking R_C into account is necessary.

To verify the accuracy of the mobility model (7), we first extract the field-effect mobility from (8) as the dotted line in Fig. 5(a) where the experimental data is from [29]. After fitting the model parameters in (6) with μ_{m1} and applying the hopping mobility model to the drain current model (17), the model results without considering R_C (the dotted in Fig. 5(b)) are a little larger than the experiment data when V_{gs} is high. Therefore, it is necessary to consider the contact resistance. Following (9), the extracted mobility (μ_m)

$$\begin{cases} h_1(\varphi_s) = \frac{qN_2\varepsilon_s}{2C_{ox}} N_1 \exp\left(\frac{\varphi_s}{\phi_1\phi_t/(\phi_1+\phi_t)}\right) \\ \qquad \div \left\{ \begin{array}{l} (N_1\phi_1)^2\left(\frac{1}{\phi_t}-\frac{1}{2\phi_1}\right)^2 \frac{1}{\phi_t{}^2}\exp\left(\frac{\varphi_s}{\phi_1/2}\right) + (N_2\phi_2)^2\left(\frac{1}{\phi_t}-\frac{1}{2\phi_2}\right)^2 \times \left(\frac{1}{\phi_t}+\frac{1}{\phi_1}-\frac{1}{\phi_2}\right)^2 \exp\left(\frac{\varphi_s}{\phi_2/2}\right) \\ +N_1\phi_1N_2\phi_2 \times \left[\left(\frac{1}{\phi_t}-\frac{1}{2\phi_1}\right)^2 + \left(\frac{1}{\phi_t}-\frac{1}{2\phi_2}\right)^2\right] \times \left(\frac{1}{\phi_t}+\frac{1}{2\phi_1}-\frac{1}{2\phi_2}\right)^2 \times \exp\left(\frac{\varphi_s}{\phi_1\phi_2/(\phi_1+\phi_2)}\right) \end{array} \right\}^{1/2} \\ I_{Deep} = \frac{W}{L}\left[\mu_{eff}(\varphi_{sd})h_1(\varphi_{sd}) - \mu_{eff}(\varphi_{ss})h_1(\varphi_{ss})\right] \end{cases} \tag{18}$$

$$\begin{cases} h_2(\varphi_s) = \frac{qN_2\varepsilon_s}{2C_{ox}} N_2 \exp\left(\frac{\varphi_s}{\phi_2\phi_t/(\phi_2+\phi_t)}\right) \\ \qquad \div \left\{ \begin{array}{l} (N_2\phi_2)^2\left(\frac{1}{\phi_t}-\frac{1}{2\phi_2}\right)^2 \frac{1}{\phi_t{}^2}\exp\left(\frac{\varphi_s}{\phi_2/2}\right) + (N_1\phi_1)^2\left(\frac{1}{\phi_t}-\frac{1}{2\phi_1}\right)^2 \times \left(\frac{1}{\phi_t}+\frac{1}{\phi_2}-\frac{1}{\phi_1}\right)^2 \exp\left(\frac{\varphi_s}{\phi_1/2}\right) \\ +N_1\phi_1N_2\phi_2 \times \left[\left(\frac{1}{\phi_t}-\frac{1}{2\phi_1}\right)^2 + \left(\frac{1}{\phi_t}-\frac{1}{2\phi_2}\right)^2\right] \times \left(\frac{1}{\phi_t}+\frac{1}{2\phi_2}-\frac{1}{2\phi_1}\right)^2 \times \exp\left(\frac{\varphi_s}{\phi_1\phi_2/(\phi_1+\phi_2)}\right) \end{array} \right\}^{1/2} \\ I_{Tail} = \frac{W}{L}\left[\mu_{eff}(\varphi_{sd})h_2(\varphi_{sd}) - \mu_{eff}(\varphi_{ss})h_2(\varphi_{ss})\right] \end{cases} \tag{19}$$

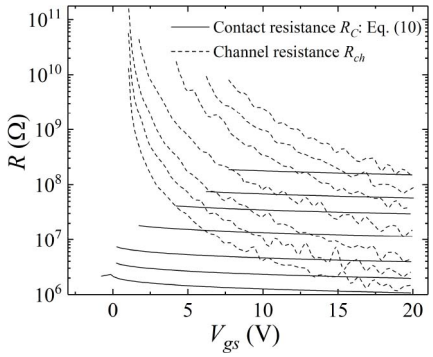

FIGURE 4. The plot of $R_C \sim V_{gs}$ at different temperatures.

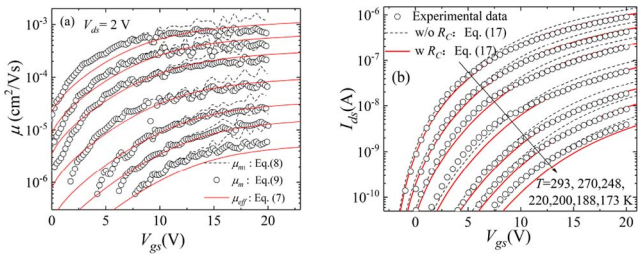

FIGURE 5. (a) Plot of μ versus V_{gs}. Dotted lines: μ_{m1} without R_C. Circle: μ_m considering R_C. (b) Plot of $I_{ds} \sim V_{gs}$ for the PTV TFT [29] at different temperatures.

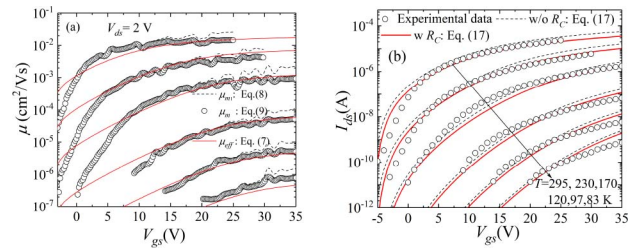

FIGURE 6. Plots of (a) μ versus V_{gs} and (b) $I_{ds} \sim V_{gs}$ for OTFTs at different temperatures [30].

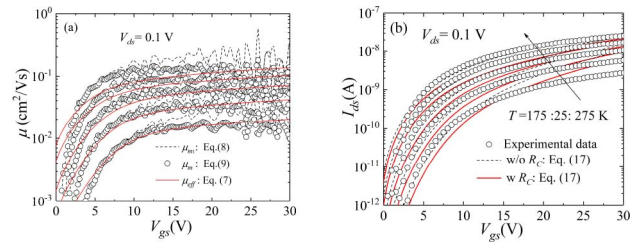

FIGURE 7. Plots of (a) μ versus V_{gs} and (b) $I_{ds} \sim V_{gs}$ for OTFTs at different temperatures [31].

is shown as the circle in Fig. 5(a). By making the fitting parameters in Eq. (6) consistent with the extracted mobility (μ_m), the mobility model (7) considering the contact resistance is plotted by solid lines. It can be clearly seen that the modeled results show a good agreement with μ_m at different temperatures. Finally, the drain current model is obtained considering contact resistance, as shown in Fig. 5(b) which suits well with the experimental data at different temperatures. All the mobility and drain current parameters are summarized in Table 1.

We have also verified the effectiveness of our model by using the samples described in [30]–[31]. As depicted in Figs. 6 and 7, the current model fits well with the experimental data. It indicates that the availability of the mobility and drain current models.

VI. CONCLUSION

In summary, this paper has presented a compact mobility model for OTFTs accounting for the mobility dependence of temperature and surface potential. Furthermore, it also takes the contact resistance into account. Assuming that the trapped carrier concentration dominates Poisson's equation, an analytical drain model expression considering both deep and tail DOS is obtained. The expression is valid in both the subthreshold and above-threshold regimes at different temperatures. A nice agreement between the model results and experimental data justifies the precise of these models.

REFERENCES

[1] O. Marinov, M. J. Deen, U. Zschieschang, and H. Klauk, "Organic thin-film transistors: Part I—Compact DC modeling," *IEEE Trans. Electron Devices*, vol. 56, no. 12, pp. 2952–2961, Dec. 2009.

[2] T. Minamiki *et al.*, "Accurate and reproducible detection of proteins in water using an extended-gate type organic transistor biosensor," *Appl. Phys. Lett.*, vol. 104, no. 24, pp. 1–4, Jun. 2014.

[3] S. Reineke *et al.*, "White organic light-emitting diodes with fluorescent tube efficiency," *Nature*, vol. 459, no. 7244, pp. 234–238, May 2009.

[4] L. Li, G. Meller, and H. Kosina, "Carrier concentration dependence of the mobility in organic semiconductors," *Synth. Metals*, vol. 157, nos. 4–5, pp. 243–246, Mar. 2007.

[5] N. F. Mott, "Conduction in glasses containing transition metal ions," *J. Non Crystalline Solids*, vol. 1, no. 1, pp. 1–17, Dec. 1968.

[6] G. Horowitz, R. Hajlaoui, and P. Delannoy, "Temperature dependence of the field-effect mobility of sexithiophene. Determination of the density of traps," *J. de Physique III*, vol. 5, no. 4, pp. 355–371, Apr. 1995.

[7] P. Servati, A. Nathan, and G. A. J. Amaratunga, "Generalized transport-band field-effect mobility in disordered organic and inorganic semiconductors," *Phys Rev. B, Condens. Matter*, vol. 74, no. 24, Dec. 2006, Art. no. 245210.

[8] T. K. Maiti, T. Hayashi, L. Chen, M. Miura-Mattausch, and H. J. Mattausch, "Organic thin-film transistor compact model with accurate charge carrier mobility," in *Proc. Int. Conf. Simulat. Semicond. Process. Devices (SISPAD)*, Oct. 2014, pp. 133–136, doi: 10.1109/SISPAD.2014.6931581.

[9] T. K. Maiti *et al.*, "A surface potential based organic thin-film transistor model for circuit simulation verified with DNTT high performance test devices," *IEEE Trans. Semicond. Manuf.*, vol. 27, no. 2, pp. 159–168, May 2014.

[10] T. K. Maiti, L. Chen, H. Zenitani, H. Miyamoto, M. Miura-Mattausch, and H. J. Mattausch, "Physically based compact mobility model for organic thin-film transistor," *IEEE Trans. Electron Devices*, vol. 63, no. 5, pp. 2057–2065, May 2016.

[11] S. Kim, T. J. Ha, P. Sonar, and A. Dodabalapur, "Charge transport in deep and shallow states in a high-mobility polymer FET," *IEEE Trans. Electron Devices*, vol. 63, no. 3, pp. 1254–1259, Mar. 2016.

[12] C. Liu *et al.*, "A unified understanding of charge transport in organic semiconductors: The importance of attenuated delocalization for the carriers," *Mater. Horizons*, vol. 4, no. 4, pp. 608–618, Mar. 2017.

[13] C. Liu *et al.*, "Device physics of contact issues for the overestimation and underestimation of carrier mobility in field-effect transistors," *Phys. Rev. Appl.*, vol. 8, no. 3, pp. 1–10, Sep. 2017.

[14] M. Fayez, K. M. Morsi, and M. N. Sabry, "OTFTs compact models: Analysis, comparison, and insights," *IET Circuits Devices Syst.*, vol. 11, no. 5, pp. 409–420, Sep. 2017.

[15] M. Shur and M. Hack, "Physics of amorphous silicon based alloy field-effect transistors," *J. Appl. Phys.*, vol. 55, no. 10, pp. 3831–3842, May 1984.
[16] W. Brütting and C. Adachi, *Physics of Organic Semiconductors*. New York, NY, USA: Wiley, Oct. 2012.
[17] J. Fang, W. Deng, X. Ma, J. Huang, and W. Wu, "A surface-potential-based DC model of amorphous oxide semiconductor TFTs including degeneration," *IEEE Electron Dev. Lett.*, vol. 38, no. 2, pp. 183–186, Feb. 2017.
[18] M. C. J. M. Vissenberg and M. Matters, "Theory of the field-effect mobility in amorphous organic transistors," *Phys. Rev. B, Condens. Matter.*, vol. 57, no. 20, pp. 12964–12967, May 1998.
[19] R. Rodel *et al.*, "Contact properties of high-mobility, airstable, low voltage organic n-channel thin-film transistors based on a naphthalene tetracarboxylic diimide," *Appl. Phys. Lett.*, vol. 102, no. 23, Jun. 2013, Art. no. 233303.
[20] M. D. Jacunski, M. S. Shur, A. A. Owusu, T. Ytterdal, M. Hack, and B. Iniguez, "A short-channel DC SPICE model for polysilicon thin-film transistors including temperature effects," *IEEE Trans. Electron Devices*, vol. 46, no. 6, pp. 1146–1158, Jun. 1999.
[21] F. Torricelli *et al.*, "Unified drain-current model of complementary *p*- and *n*-type OTFTs," *Org. Electron.*, vol. 22, pp. 5–11, Jul. 2015.
[22] L. Li, H. Marien, J. Genoe, M. Steyaert, and P. Heremans, "Compact model for organic thin-film transistor," *IEEE Electron Devices Lett.*, vol. 31, no. 3, pp. 210–212, Mar. 2010.
[23] Y. Liu, H. He, R. Chen, Y. F. En, B. Li, and Y. Q. Chen, "Analysis and simulation of low-frequency noise in indium-zinc-oxide thin-film transistors," *IEEE J. Electron Devices Soc.*, vol. 6, no. 1, pp. 271–279, Jan. 2018.
[24] F. Yu, C. Xu, G. Huang, W. Lin, and T. C. Liang, "A closed-form trapped-charge-included drain current compact model for amorphous oxide semiconductor thin-film transistors," *Microelectron. Rel.*, vol. 91, pp. 307–312, Dec. 2018.
[25] W. Deng, J. Huang, and X. Li, "Surface-potential-based drain current model of polysilicon TFTs with Gaussian and exponential DOS distribution," *IEEE Trans. Electron Devices*, vol. 59, no. 1, pp. 94–100, Jan. 2012.
[26] H. He, Y. Liu, B. Yan, X. Lin, X. Zheng, and S. Zhang, "Analytical drain current model for organic thin-film transistors at different temperatures considering both deep and tail trap states," *IEEE Trans. Electron Devices*, vol. 63, no. 11, pp. 4423–4431, Nov. 2016.
[27] L. Colalongo, "SQM-OTFT: A compact model of organic thin-film transistors based on the symmetric quadrature of the accumulation charge considering both deep and tail states," *Org. Electron.*, vol. 32, pp. 70–77, May 2016.
[28] C. Liu *et al.*, "Universal diffusion-limited injection and the hook effect in organic thin-film transistors," *Sci. Rep.*, vol. 6, pp. 1–14, Jul. 2016.
[29] C. Tanase, P. W. M. Blom, E. J. Meijer, and D. M. de Leeuw, "Charge transport in disordered organic field-effect transistors," *Meter. Res. Soc.*, vol. 725, pp. 125–129, Apr. 2002. doi: 10.1557/PROC-725-P10.9.
[30] W. S. C. Roelofs, S. G. J. Mathijssen, R. A. J. Janssen, D. M. de Leeuw, and M. Kemerink, "Accurate description of charge transport in organic field effect transistors using an experimentally extracted density of states," *Phys. Rev. B, Condens. Matter*, vol. 85, no. 8, Feb. 2012, Art. no. 085202.
[31] L. Mariucci *et al.*, "Contact effects in organic thin film transistors with different device structures," *ECS Trans.*, vol. 64, no. 10, pp. 131–142, 2014.

NA LI received the B.S. degree from the Hubei University of Education, Wuhan, China, in 2017. She is currently pursuing the M.S. degree with Jinan University, Guangzhou, China.

Her current research interest includes the modeling of the organic thin-film transistors.

WANLING DENG received the B.S. and Ph.D. degrees in electrical engineering from the South China University of Technology, Guangzhou, China, in 2003 and 2008, respectively.

Since 2008, she has been an Associate Professor with the Department of Electronic Engineering, Jinan University, Guangzhou. Her current research interests include thin-film transistor (TFT) devices and physics, particularly poly-Si TFT and AOS TFT modeling.

WEIJING WU was born in Fuzhou, China. He received the Ph.D. degree from the South China University of Technology, Guangzhou, China, in 2008.

In 2008, he joined the Institute of Polymer Optoelectronic Materials and Devices, South China University of Technology, where he is currently an Associate Professor with the State Key Laboratory of Luminescent Materials and Devices. His current research interests include thin-film transistors and AMOLED displays.

ZHI LUO received the Ph.D. degree from Hong Kong University, Hong Kong, in 2009.

Since 2011, he has been an Associate Professor with the Department of Electronic Engineering, Jinan University, Guangzhou. His current research interests include new materials and devices.

JUNKAI HUANG received the B.S. degree in applied physics and the M.S. degree in semiconductor device from Jinan University, Guangzhou, China, in 1985 and 1990, respectively, and the Ph.D. degree from the Institute of Microelectronics, South China University of Technology, Guangzhou, in 2011.

He is currently a Professor with Jinan University. His current research interests include thin-film transistors' modeling, simulation, and integrated circuit design.